Solid Earth, 12, 1125–1142, 2021
https://doi.org/10.5194/se-12-1125-2021

Solid Earth Open Access EGU

Application of anisotropy of magnetic susceptibility (AMS) fabrics to determine the kinematics of active tectonics: examples from the Betic Cordillera, Spain, and the Northern Apennines, Italy

David J. Anastasio[1], Frank J. Pazzaglia[1], Josep M. Parés[2], Kenneth P. Kodama[1], Claudio Berti[3], James A. Fisher[1], Alessandro Montanari[4], and Lorraine K. Carnes[5]

[1]Department of Earth and Environmental Sciences, Lehigh University, Bethlehem, PA 18015, USA
[2]Geochronology, Centro Nacional de Investigación de la Evolución Humana (CENIEH) Burgos, Burgos, 09002, Spain
[3]Idaho Geological Survey, Moscow, ID 83844, USA
[4]Osservatorio Geologico di Coldigioco, Apiro, Macerata, 62021, Italy
[5]Geological Sciences, Arizona State University, Tempe, AZ 85281, USA

Correspondence: David J. Anastasio (dja2@lehigh.edu)

Received: 29 October 2020 – Discussion started: 20 January 2021
Revised: 23 March 2021 – Accepted: 7 April 2021 – Published: 19 May 2021

Abstract. The anisotropy of magnetic susceptibility (AMS) technique provides an effective way to measure fabrics and, in the process, interpret the kinematics of actively deforming orogens. We collected rock fabric data of alluvial fan sediments surrounding the Sierra Nevada massif, Spain, and a broader range of Cenozoic sediments and rocks across the Northern Apennine foreland, Italy, to explore the deformation fabrics that contribute to the ongoing discussions of orogenic kinematics. The Sierra Nevada is a regional massif in the hinterland of the Betic Cordillera. We recovered nearly identical kinematics regardless of specimen magnetic mineralogy, structural position, crustal depth, or time. The principal elongation axes are NE–SW in agreement with mineral lineations, regional GPS geodesy, and seismicity results. The axes trends are consistent with the convergence history of the Africa–Eurasia plate boundary. In Italy, we measured AMS fabrics of specimens collected along a NE–SW corridor spanning the transition from crustal shortening to extension in the Northern Apennines. Samples have AMS fabrics compatible only with shortening in the Apennine wedge and have locked in penetrative contractional fabrics, even for those samples that were translated into the actively extending domain. In both regions, we found that specimens have a low degree of anisotropy and oblate susceptibility ellipsoids that are consistent with tectonic deformation superposed on compaction fabrics. Collectively, these studies demonstrate the novel ways that AMS can be combined with structural, seismic, and GPS geodetic data to resolve orogenic kinematics in space and time.

1 Introduction

A number of circum-Mediterranean orogens are associated with rapid slab rollback, resulting in paired compressional and extensional domains in the orogenic wedge of the retreating upper plate (Elter, 1975; Carminati and Doglioni, 2012). Examples include the Calabria Arc–Tyrrhenian Sea (Beccaluva et al., 1985; Milia et al., 2009), the Hellenic Arc–Aegean Sea (Le Pichon and Angelier, 1979; Papazachos et al., 2000), and the Gibraltar Arc–Alboran Sea (Lonergan and White, 1997; Platt et al., 2006; Fernández-Ibáñez and Soto, 2008). Along these tectonic boundaries, the temporal and spatial relationship between thrust belt contraction, wedge-top basin evolution, hinterland extension, and orogenic uplift are the subjects of continuing controversy.

Finite and incremental strain data provide deformation history and fabric distribution information for kinematic studies of folds, faults, and orogens (e.g., Ramsay and Huber, 1984; Fagereng and Biggs, 2018). However, in orogenic forelands where deformation occurs at shallow depths and low temperatures, ductile penetrative deformation features may be

absent and brittle structures may be sparse. Anisotropy of magnetic susceptibility (AMS) results offers an alternative proxy for grain-preferred orientation, and hence rock strain, to determine the tectonic fabric in these orogens where other deformation markers are not available (Borradaile and Jackson, 2004, 2010; Borradaile and Henry, 1997; Averbuch et al., 1992; Parés, 2004). In general, comparative studies from siliciclastic rocks show good agreement between both the relative magnitude and orientation of penetrative rock strain determined by traditional geometric methods and AMS principal axes; however, in specimens dominated by diamagnetic mineral abundance, the AMS axes' orientation, and not necessarily their magnitude, correlates to the rock strain (e.g., Latta and Anastasio, 2007; Burmeister et al., 2009). In this paper, we show how AMS can extend the temporal reach of GPS geodesy back in time in orogenic studies of the Betic Cordillera, Spain, and in the Northern Apennines, Italy (e.g., Sagnotti et al., 1998; Mattei et al., 2004; Fig. 1).

2 Kinematic studies for active tectonic research

Sedimentary rocks acquire a primary depositional fabric, which is bedding parallel. It is measurable with the AMS technique and is further enhanced and modified during burial, compaction, and water loss (e.g., Tarling and Hrouda, 1993; Schwehr et al., 2006). Even unconsolidated rocks record a magnetic fabric that can potentially provide a kinematic record (Mattei et al., 1997; Porreca and Mattei, 2012). The sensitivity of AMS allows its use as a paleogeodetic tool in tectonic studies. Kinematics allow for an assessment of rheology and strain history that are necessary prerequisites for understanding geodynamics, incrementally balancing cross sections, or in paleogeographic reconstructions. We sampled both consolidated sedimentary rocks and unconsolidated sediments in the Betic Cordillera, Spain, and northeastern Apennine ranges, Italy, for AMS analysis. The Betics field sampling was designed to test AMS recovery from unburied and unconsolidated sediments around the Sierra Nevada massif. Here, oriented samples were collected from sites around the Sierra Nevada massif in Plio-Pleistocene terrestrial, siliciclastic deposits (Table A1 in Appendix). The Apennines field sampling was designed to measure the rotation of strain across the foreland as sampling site passes from the actively shortening part of the orogenic wedge near the trench to the actively extending regime further to the southwest. Here, oriented samples were collected from sites along a NE–SW-oriented corridor inclusive of Cenozoic marine and fluvial siliciclastics, marls, and carbonate rocks, and unconsolidated Pleistocene fluvial sediments (Table A1).

3 The AMS method

The AMS ellipsoid is defined by the principal axes (k_1 – maximum, k_2 – intermediate, k_3 – minimum) of a specimen. It can be represented by a second-rank tensor that characterizes a material's magnetization response to an applied magnetic field (e.g., Borradaile and Tarling, 1981; Tarling and Hrouda, 1993). The orientation and relative length of the principal anisotropy axes of a specimen are controlled by the preferred alignment of the anisotropy axes of the individual magnetic particles in the specimen and the degree of the individual particle's anisotropy. The anisotropy of individual magnetic grains is controlled by their crystallography and grain shape (Tarling and Hrouda, 1993). For magnetite grains, the anisotropy is controlled by grain shape, whereas for hematite and phyllosilicate particles the anisotropy can be controlled by a grain's crystallography, which, in turn, controls their shape. This does not preclude the possibility of the mutual orientation of different particles (e.g., Housen et al., 1993; Weil and Yonkee, 2009) or the preferential alignment of iron-bearing inclusions within the particles (e.g., Biedermann, 2018; Borradaile and Werner, 1994; Borradaile and Lagroix, 2000; Martín-Hernandez and Hirt, 2003; Parés and van der Pluijm, 2002) controlling the AMS fabric.

Natural processes such as current deposition, lithification, and tectonic deformation all contribute to a specimen's AMS. In deformed rocks, it was shown that the principal susceptibility axis (k_1) orientation is typically parallel to the strain long axis and orthogonal to the tectonic shortening direction, whereas the shortest axis (k_3) is orthogonal to bedding in orientation (e.g., Kligfield et al., 1981; Hrouda, 1982), regardless of whether the individual particle anisotropy is controlled by crystallography or shape.

The sedimentary rocks and deposits in this study contain enough phyllosilicate minerals to be excellent specimens for AMS studies because of the presence of oblate mineral grains which adjust readily to deposition, lithification, and any subsequent deformation. As grains reorient in response to depositional or tectonic processes, the magnetic fabric will continuously adjust (Parés and van der Pluijm, 2002). Deposition from currents in alluvial fans or rivers like the examples discussed here can cause preferred grain alignment. Because the intermediate and maximum AMS axes of platy grains, such as phyllosilicates, are nearly equal in magnitude, they will be randomly oriented within the bedding plane, with the minimum axes orthogonal to bedding. In mudstones and fine-grained sandstones, where both paramagnetism and ferromagnetism contributions were quantified, paramagnetic mineral grains typically dominate the AMS signal (e.g., Martín-Hernández and Hirt, 2001) because of the shape anisotropy of clay minerals, although very fine magnetic particles attached to the clay fabric might also contribute (Kodama and Sun, 1992). Clustering of k_1 axes (magnetic lineation) under progressive deformation has been observed in a number of studies and is occasionally accompanied by a girdle containing k_3 and k_2 axes. This particular axes distribution is thought to be the first piece of evidence for layer parallel shortening in sedimentary rocks (Kissel et al., 1986; Sagnotti and Speranza, 1993; Parés and Dinarès, 1993; Sagnotti

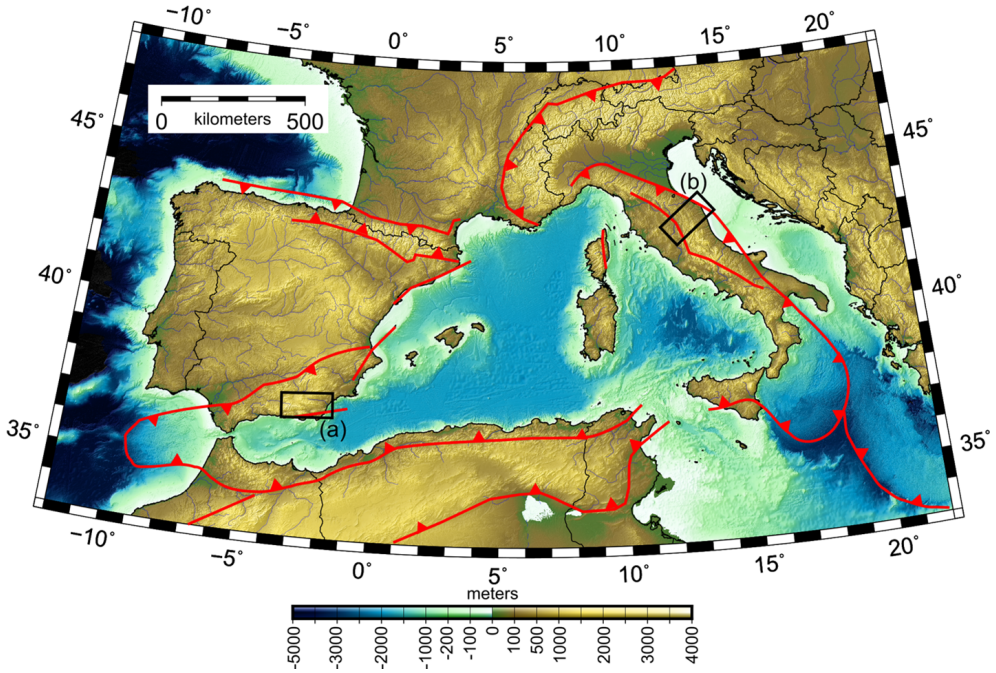

Figure 1. Topography and bathymetry of the western Mediterranean showing **(a)** the Betic orogen, southern Spain, and **(b)** the Northern Apennine mountains, Italy. Elevation data are from General Bathymetric Chart of the Oceans (GEBCO) 30 s data (https://www.gebco.net/data_and_products/gridded_bathymetry_data/, last access: 8 May 2021).

et al., 1994; Parés et al., 1999) in sequences of low to moderately deformed mudstones. Borradaile (1988) had already described that the intersection of two competing fabrics (e.g., bedding and layer parallel shortening) will control the orientation of the k_1 direction, producing an intersection lineation or magnetic lineation. The concept of magnetic lineation as a result of an assemblage of clay minerals (platelets) was originally brought up by Henry (1997), who referred to it as the "zone axis of two planar objects", a concept that was reviewed by Parés and van der Pluijm (2002).

4 Example I: Sierra Nevada massif, Spain

4.1 Geologic setting of the Sierra Nevada massif

The Sierra Nevada massif is part of the Betic Cordillera–Rif–Tell orogens that extend along the European–African plate boundary from the southern Iberian Peninsula to northern Africa. These orogens were formed by slab rollback and western migration of the Gibraltar Arc throughout the Neogene (Rosenbaum et al., 2002). Coincident with the translation of the arc, the upper plate experienced shortening, the growth of doubly vergent thrust belts, crustal thickening, and rock uplift (Duggen et al., 2003; Soto et al., 2008; Platt et al., 2013). In the Betics, contraction across the plate boundary was initially directed northward (Sanz De Galdeano, 1990; Lonergan, 1993; Platt et al., 2013). As the contraction continued into the foreland during the late Miocene, it slowed and progressively rotated to the northwest into its present orientation (Mazzoli and Helman, 1994; Rosenbaum et al., 2002). Active tectonics in the Betic Cordillera today is dominated by distributed NW–SE convergence of 4–6 mm yr^{-1} (Fernández-Ibanez et al., 2007; Koulali et al., 2011; Gutscher et al., 2012; Mancilla et al., 2013) and is accommodated in part on NW–SE-trending normal faults (Martínez- Martínez et al., 2006; Stich et al., 2006; Fernández-Ibáñez and Soto, 2008; Giaconia et al., 2014, 2015; Fig. 2).

The Sierra Nevada massif is a doubly plunging, actively uplifting (Azañón et al., 2015) elongate dome, characterized by medium to low-grade metamorphic rocks stacked in north-verging thrust sheets (Martínez-Martínez et al., 2002). Previous interpretations are that the Sierra Nevada dome was uplifted following top-to-west extension and isostatic rebound after thrust belt formation (Martínez-Martínez et al., 2006). Alternatively, as many culminations exist in orogenic hinterlands, the massif could have been uplifted during contractional or transpressive strain (e.g., Bernini, 1990; Mitra et al., 1997).

To resolve whether the uplift of the Sierra Nevada dome was the result of extensional exhumation or a compressional orogenic culmination, we collected rock fabric (AMS) data in Plio-Pleistocene deposits around the massif to explore the presence of penetrative tectonic fabrics that can contribute additional constraints to the kinematics of dome emplacement. We focused sampling on unburied alluvial fan deposits

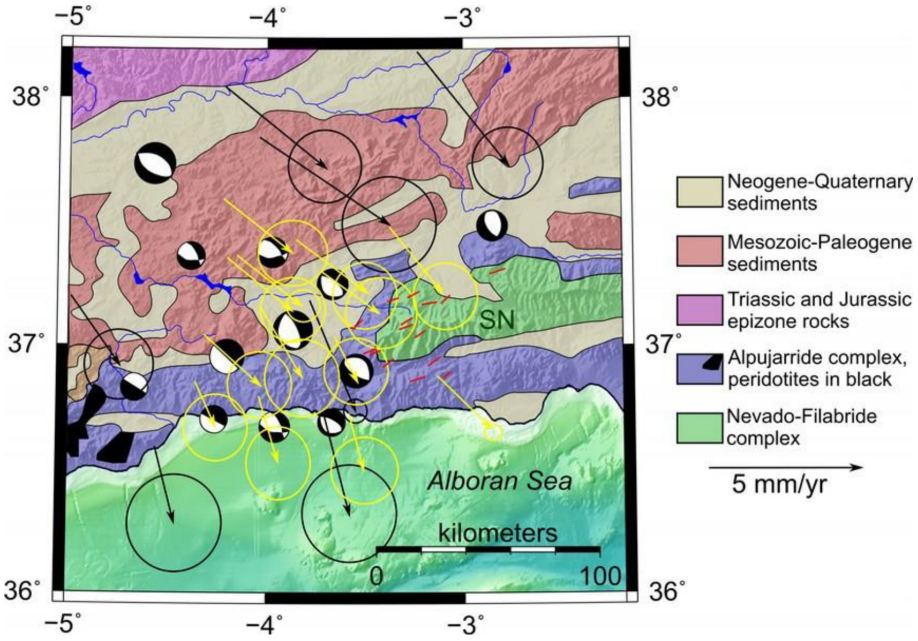

Figure 2. Geodetic, paleogeodetic, and earthquake focal mechanism data from southern Spain. Generalized geology (from Azañon et al., 2015), focal mechanism solutions for normal faults (from Mancilla et al, 2013; earthquake locations from International Seismological Centre catalogue, http://www.ics.ac.uk/, last access: 8 May 2021), mineral lineations (short red lines) (from Martínez-Martínez et al., 2002), results from 10 years of observed velocity GPS permanent (black arrows, with uncertainties) (from Gutscher et al., 2012), and campaign (yellow arrows and uncertainties) (from Koulali et al., 2011) stations in an African (Nubian) fixed reference frame. SN indicates the Sierra Nevada. Bathymetry color depths are as in Fig. 1. Elevation data are from the 30 m NASA Shuttle Radar Topography Mission (SRTM) Jet Propulsion Laboratory (JPL) combined image data set 2014, distributed by NASA EOSDIS Land Processes DAAC (https://doi.org/10.5067/MEaSUREs/SRTM/SRTMIMGM.003).

in Neogene basins that surround the core of the structure (Fig. 3).

4.2 Methods for Example I

We collected samples from six sites distributed around Sierra Nevada, from all structural positions, around the massif in unburied Plio-Pleistocene fan deposits that range from poorly cemented to unconsolidated (Sanz de Galdeano and Vera, 1992; Table A1; Fig. 3). The ages of the deposits sampled were determined from published geologic maps (IGME-1 : 50 000 scale) and bridged the temporal gap between the late Miocene age metamorphic fabrics and the present-day deformation field recorded by GPS geodesy and recent seismicity. At each site, three oriented samples were collected as independent blocks. Before removal from the outcrop, most blocks were hardened with a diluted ($\sim 50\,\%$) aqueous solution of sodium silicate (Fig. 4). In the laboratory, two to three oriented cubes ($8\,cm^3$) were cut from each block using non-magnetic Teflon knives and enclosed in standard cubic paleomagnetic boxes. The anisotropy of magnetic susceptibility (AMS) was determined with an Agico KLY-3S Kappabridge at Lehigh University. To determine magnetic mineralogy, a heating stage under the presence of an argon atmosphere and a cold stage accessory to the Kappabridge were used.

4.3 Results for Example I

Results from heating and cooling experiments show a complicated magnetic mineralogy composed of nearly 100 % ferromagnetic (magnetite or hematite) to nearly 100 % paramagnetic mineralogy (clays and iron-rich micas; Fig. 5). Since the kinematic interpretation of each of the specimen is the same regardless of magnetic mineralogy, the details of each specimen are not important for subsequent analysis. There is no correlation between the bulk magnetic susceptibility (k_m) and the anisotropy of the magnetic ellipsoid (P_j), so a comparison of the principal axis of susceptibility across the various structural positions around the Sierra Nevada massif specimens can provide useful kinematic information (Fig. 6a). Site 6 has a much higher magnetic susceptibility than the other sites because of possible secondary sulfide minerals at the site indicated by the heating and cooling behavior of the MS vs. T experiments.

Nearly all AMS ellipsoids are characterized by a low anisotropy degree (P_j) and oblate ellipsoid shape (T) (Jelinek, 1981; Fig. 6b). The AMS axes' determinations record nearly the same axis orientations. At all sites around the Sierra Nevada, the minimum principal axes, k_3, are nearly orthogonal to bedding. The principal elongation axes means are preferentially oriented NNE–SSW to NE–SW (Fig. 3).

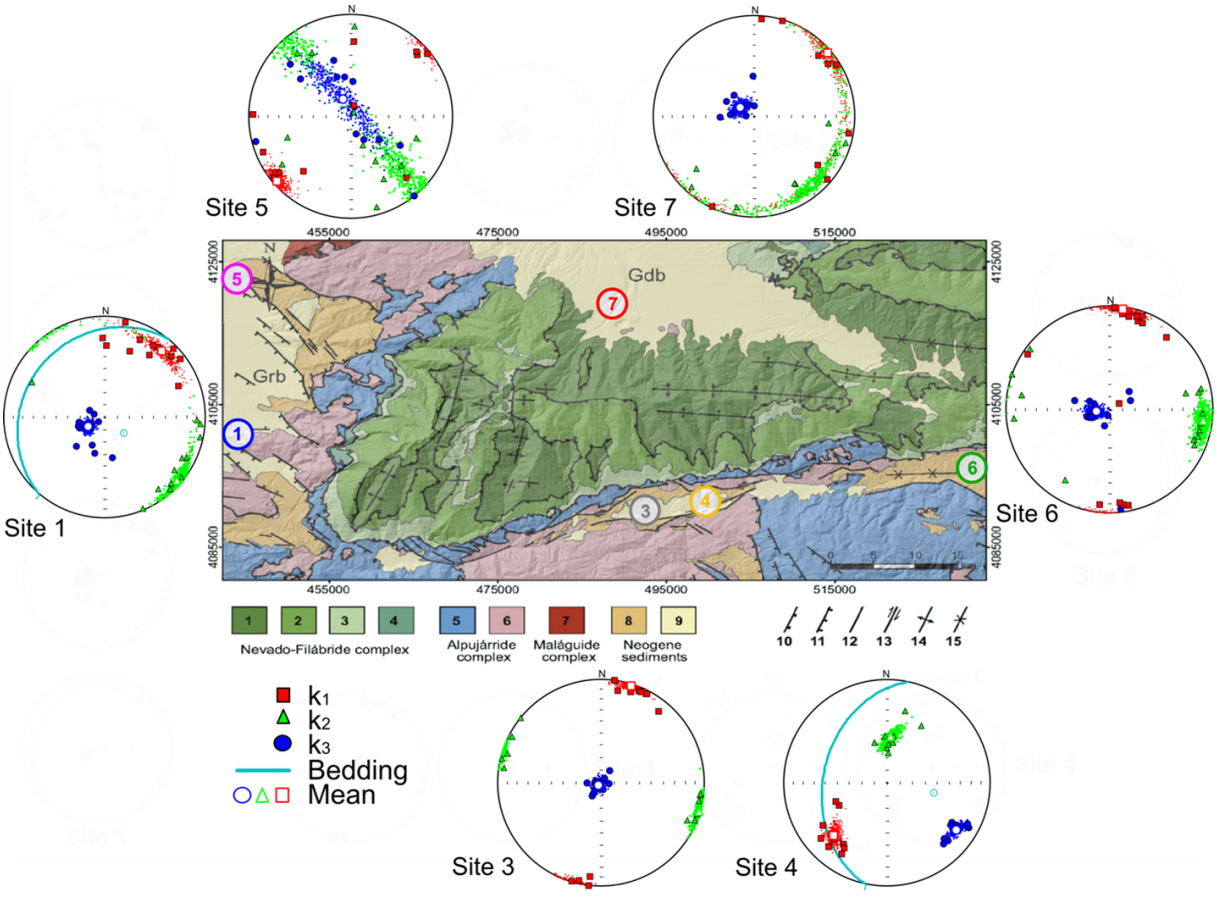

Figure 3. Simplified geologic map showing sample sites around the Sierra Nevada massif, southern Spain. Lithostructural map of the study area (modified from Azañon et al., 2015). Nevado-Filábride Complex: (1) Ragua unit, (2) and (3) Calar Alto unit, Paleozoic and Permo-Triassic rocks, respectively, and (4) Bédar-Macael unit. Alpujárride Complex: (5) Lújar-Gádor unit and (6) upper Alpujárride units. Malaguide Complex: (7) undifferentiated units. Neogene sediments: (8) Miocene and (9) Pliocene to Quaternary. (10) Low-angle inactive normal fault, (11) high-angle normal fault, (12) high-angle normal fault (undifferentiated), (13) strike-slip fault, (14) anticline, and (15) syncline. Gdb is the Guadix Basin and Grb is the Granada Basin. Lower hemisphere stereographic projection of AMS determined principal axes: k_1 axes are indicated by red squares, k_2 by green triangles, and k_3 by blue circles. Bedding orientation shown along with axes' orientation uncertainties. Elevation data are from the 30 m NASA SRTM JPL combined image data set 2014, distributed by NASA EOSDIS Land Processes DAAC (https://doi.org/10.5067/MEaSUREs/SRTM/SRTMIMGM.003).

Figure 4. Examples of specimen collection from poorly cemented samples. **(a)** A sampling surface is carved in a massive sandstone of the Upper Miocene Laga Fm., Northern Apennines. **(b)** The same is done on a subhorizontal layer of a poorly cemented, fine calcareous sandstone from an upper Middle Pleistocene fluvial terrace exposed in a wine cellar at the Geological Observatory of Coldigioco, Northern Apennines. Both samples were hardened with a dilute sodium silicate solution. Three or four oriented blocks were collected from each sampling site. Samples were oriented with a Brunton compass and located with a handheld GPS receiver, labeled, and photographed.

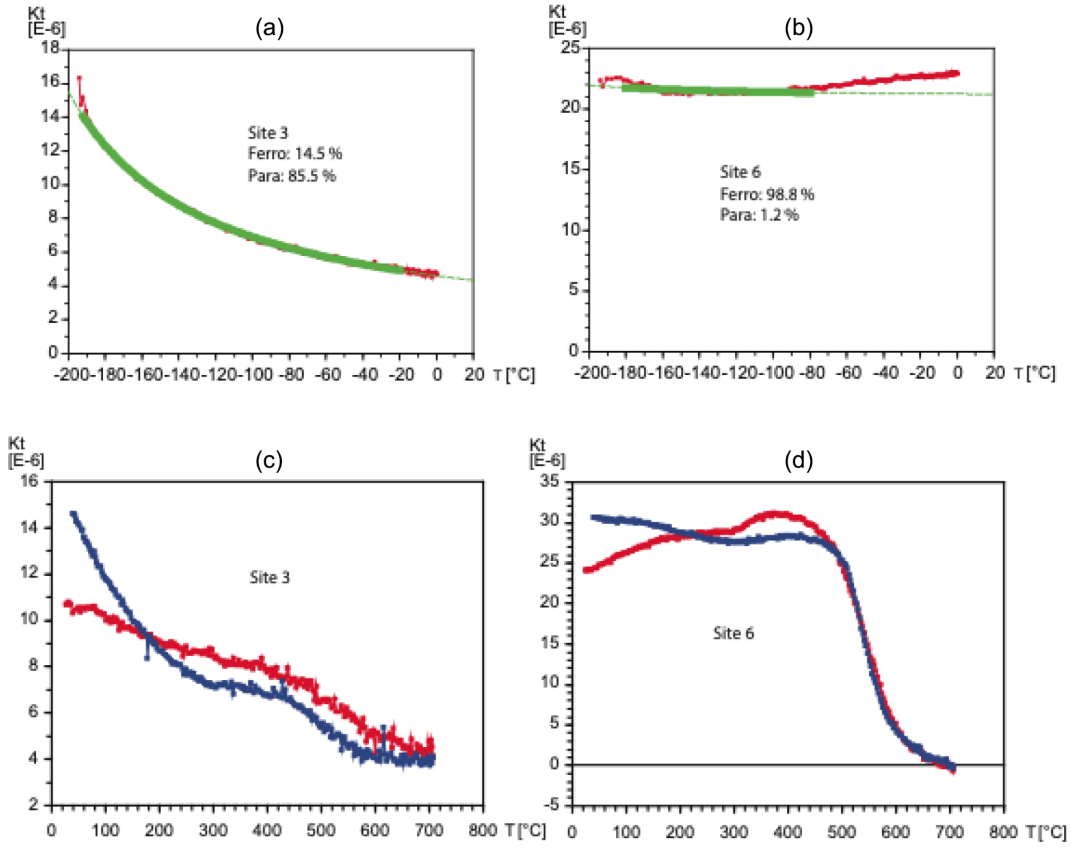

Figure 5. Magnetic mineralogy of Sierra Nevada specimens. **(a, b)** Low temperature (MS vs. T) measured on a KLY-3S Kappabridge at Lehigh University. Data are in red and paramagnetic modeling in green, indicating the proportion of the magnetic susceptibility carried by paramagnetic grains. Results from all measurements indicate that the magnetic susceptibility of the Spanish samples varies from being dominated by paramagnetic to ferromagnetic mineral grains. Irrespective of whether the greatest magnetic lineation, k_1, is controlled by grain shape of crystallography, the kinematic interpretation is the same. **(c, d)** High temperature (MS vs. T) measurements showing heating from room temperature (20 °C) to 700 °C and subsequent cooling back to room temperature. All four plots show evidence of the ferromagnetic mineral magnetite (Curie temperature of 580 °C). A lower temperature phase is indicated at Site 3, possibly maghemite. Site 6 shows the formation of additional magnetite during heating because of the much stronger susceptibility upon cooling. Heating curves are in red and cooling curves in blue.

The orientation of the site-mean magnetic susceptibility axes, k_1, is horizontal or very shallowly plunging to the NE or SW (Fig. 3). In general, k_1 and k_2 are in or near the bedding plane of the specimens, and k_2 and k_3 do not form a girdle pattern in this principle plane.

4.4 Discussion of Example I

The AMS principal axes show a consistency between sites (Fig. 3), so we combine the susceptibility axes' orientation data in Fig. 7. These combined data suggest that during deposition the phyllosilicate grains were oriented with their basal planes parallel or slightly imbricated to the depositional surface. Compaction during dewatering and lithification amplified the initial oblate depositional fabric and was coincident with the formation of the tectonic fabric. Regardless of the magnetic mineralogy of the specimens, a well-clustered minimum susceptibility axis (k_3) is present, which we interpret as a compaction fabric in these sedimentary deposits. The possibility of a primary depositional current fabric (imbrication) is unlikely because of an independent paleocurrent study on clast imbrication at Site 3 and Site 4, which shows an eastward rather than westward transport direction during deposition (Carrigan et al., 2018).

Irrespective of the structural position around the Sierra Nevada massif, all sites show a preferred orientation of k_1. The mean principal axis of maximum susceptibility is preferentially oriented at 30–210° (Figs. 7 and 8). We interpret this as a tectonic fabric due to the tight clustering of k_1 and k_2, the relationship between k_1 and strike of dipping bedding at sites SN1, SN4, and SN6, and the lack of influence from depositional processes. In specimens dominated by phyllosilicate grains, it is difficult to create a strong lineation by aligning grain crystallographic axes; however, an intersection lineation between slightly rotated clay grains orthogonal to a

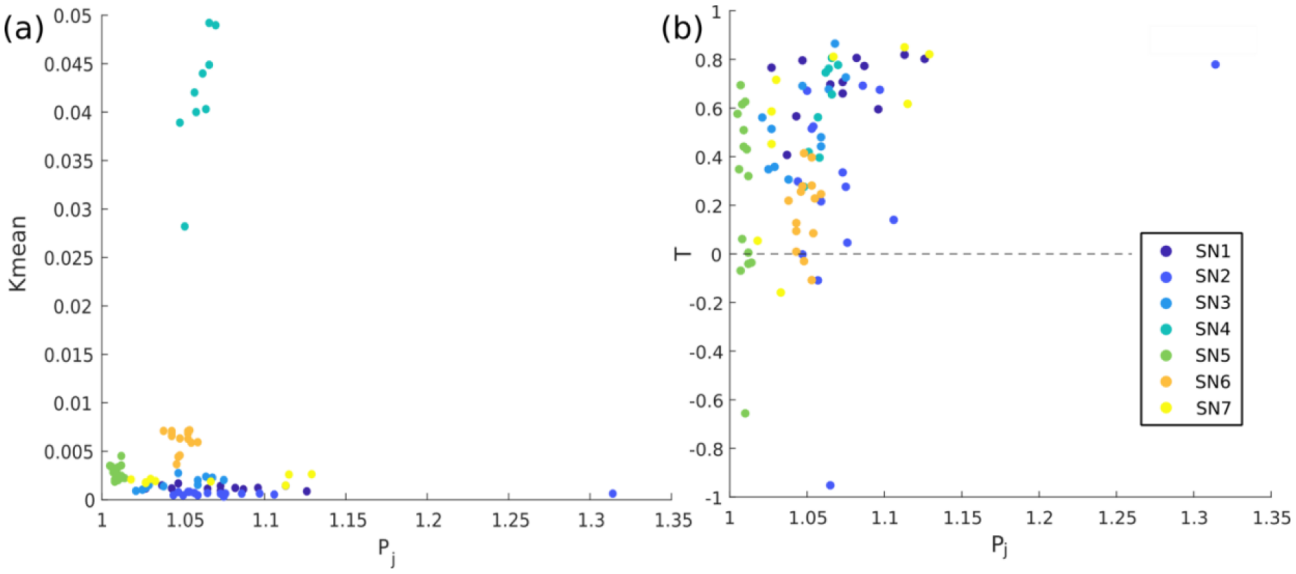

Figure 6. **(a)** Plot of mean susceptibility (K_m) with respect to ellipsoid shape (T) for Sierra Nevada samples. Oblate shapes are positive T, whereas prolate shapes are negative T. Most of the specimens have oblate AMS ellipsoid shapes. The specimens are color coded by site and consistent with Fig. 3. The lack of correlation between ellipsoid shape and susceptibility strengthen the conclusions based on the site comparisons we present here. **(b)** Jelinek diagram of Sierra Nevada specimens colored by site and consistent with Fig. 3 colors. All AMS measurement have a low anisotropy (less than 12 % P_j) and nearly all specimens are oblate ($T>0$). T and P_j are calculated as follows: if $n_1 = \ln(t_1)$, $n_2 = \ln(t_2)$, $n_3 = \ln(t_3)$, where t_1, t_2, and t_3 are the eigenvalues, then $T = (2n_2 - n_1 - n_3)/(n_1 - n_3)$ and $P' = \exp(\sqrt{(2[(n_1 - n_{mean})2 + (n_2 - n_{mean})2 + (n_3 - n_{mean})2]})$ and $n_{mean} = (n_1 + n_2 + n_3)/3$ (Jelinek, 1981).

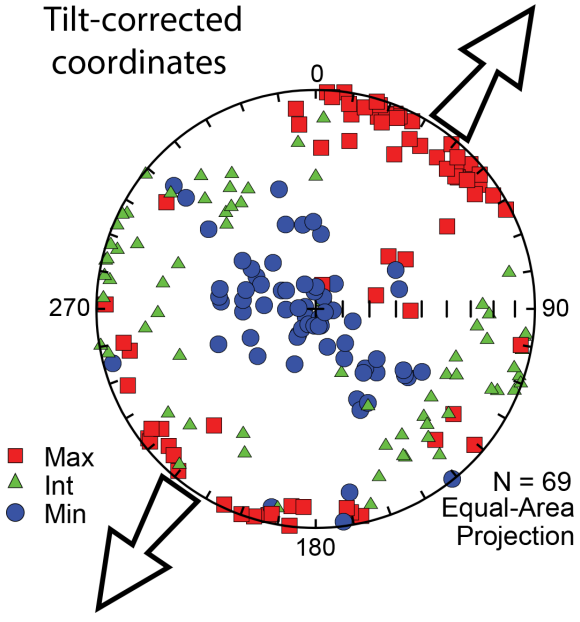

Figure 7. All Sierra Nevada massif AMS data. Lower hemisphere, stereographic projection of the principal axes of susceptibility orientations for all specimens determined from AMS measurements in tilt-corrected coordinates (Fig. 3). Arrows outside the stereonet periphery are parallel to the mean long axis (k_1) orientation. k_1 is the maximum axis, k_2 is the intermediate axis, and k_3 is the minimum axis.

shortening direction has been observed (Henry, 1997; Cifelli et al., 2004; Parés et al., 2007; Martín-Hermández and Ferré, 2007; Borradaile and Jackson, 2010). The orientation of k_1 is consistent with the present-day GPS velocity field, being oriented almost perfectly orthogonal to the direction of convergence of the Betic Cordillera to stable Africa (Nubia; Fig. 2; Gutscher et al., 2012), in good agreement with the mineral lineations recorded in the massif's core (Martínez-Martínez et al., 2002), and the Neogene brittle extensional structures and recent seismicity (Mancilla et al., 2013) in the orogen (Fig. 2). Because of the low strains and the orthogonal relationship between contractional and extensional principal directions, it is not possible to distinguish the uplift processes of the Sierra Nevada massif with our results. The AMS ellipsoid orientations, mineralogic stretching lineation from the core of the Sierra Nevada massif, the nearby GPS velocity field, and recent fault slip all have orientations consistent with the same strain field (Fig. 8). The principal elongation direction is interpreted to have persisted across different structural levels from Miocene time to the present (>10 Myr). The principal elongation direction, k_1, was collected from only young sediments so this fabric must also be young. The AMS fabric points out that the various phases of deformation affecting the Betic Cordillera were nearly coaxial since the Miocene.

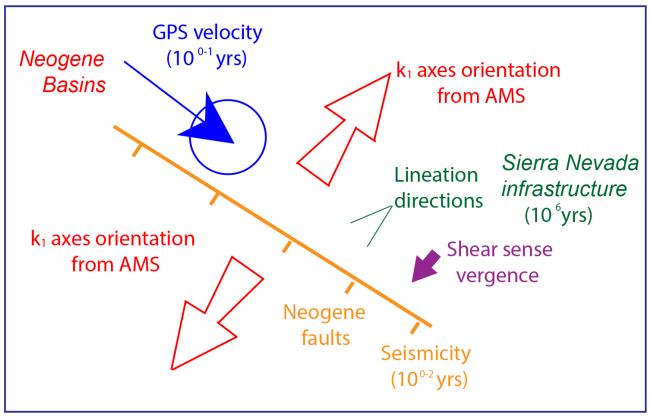

Figure 8. Kinematic summary of AMS for Example I. Comparison of paleogeodetic methods around the Sierra Nevada massif, Spain, illustrating the validity of AMS determined principal extension direction (k_1).

5 Example II: Northern Apennines, Italy

5.1 Geologic setting of the Northern Apennines

The Northern Apennines are an accretionary fold and thrust belt (Bally et al., 1986) where crustal deformation, rock uplift, and topographic growth result from the ongoing subduction of Adria beneath Europe (Picotti and Pazzaglia, 2008; Carminati and Doglioni, 2012). The Apennine orogenic wedge initiated ∼ 30 Ma along the southern flank of the Alps (Le Pichon et al., 1971) and has grown at variable rates through the Neogene dependent on the transfer of mass imbricated from the subducting plate (Picotti and Pazzaglia, 2008). Rapid rollback of Adria with respect to Europe results in retreat and stretching of the upper plate, forming a wide zone of back arc crustal extension. The Apennine wedge started to become emergent ∼ 4 Ma (Picotti and Pazzaglia, 2008), uplifting and exposing paired compressional and extensional deformation fronts near the trench and in the forearc, respectively, with the structural transition near the topographic culmination of the range (D'Agostino et al., 2001; Carminati and Doglioni, 2012). Balanced cross sections for the Apennines (Bally et al., 1986; Hill and Hayward, 1988) indicate ∼ 130 to 150 km of subduction over the 30 Myr history of the wedge, which indicates relatively slow long-term rates at ∼ 4 to 5 km Myr^{-1} (4–5 mm yr^{-1}), similar to the GPS geodetic rates (Devoti et al., 2008; Caporali et al., 2011; Bennett et al., 2012).

The northeastern Apennines, including the Umbria–Marche target region of this research, exposes Mesozoic–early Cenozoic carbonates and middle–late Cenozoic mixed carbonate–siliciclastic rocks folded and imbricated into northeast-vergent thrust sheets (Porreca et al., 2018, and references therein; Fig. 9). In Marche, these thrust sheets are located with carbonate ridges and have inferred blind thrusts in their cores (Artoni, 2013). Further west in Umbria, the thrust sheets are dissected by both east- and west-dipping high-angle normal faults (Barchi et al., 1998; Fig. 9). Ongoing thrust earthquakes beneath the Po Plain and Adriatic Sea (Pondrelli et al., 2006; Boccaletti et al., 2011) and normal-fault-sense earthquakes beneath the high Apennines (Lavecchia et al., 1994; Doglioni et al., 1999; Ghisetti and Vezzani, 2002; Chiaraluce et al., 2017) speak to concurrent shortening and extension in the wedge.

The paired deformation fronts in the Northern Apennines, Italy, are convolved with an enigmatic, but active, east-dipping (towards Adria), 14–15 km deep detachment called the Alto Tiberina fault that projects to the surface west of the Apennine crest (Barchi et al., 1998; Pialli et al., 1998; Boncio et al., 2004; Chiaraluce et al., 1999; Eva et al., 2014; Lavecchia et al., 2016; Fig. 9). This detachment is one of only a handful of low-angle normal faults globally that are demonstrably seismogenic (Hreinsdóttir and Bennett, 2009; Valoroso et al., 2017), apparently in contradiction to frictional fault reactivation theory that predicts that slip on low-angle normal faults as extremely unlikely (reviewed in Collettini, 2011). Most of the destructive seismicity in the high Apennines tends to nucleate on west-dipping high-angle normal faults that are antithetic to and sole into this east-dipping detachment (Galadini and Galli, 2000; Boncio et al., 2004; Roberts and Michetti, 2004). The most destructive seismicity, including the 2016–2017 earthquake sequence, is tightly focused along the highest crest of the Apennines where it is co-located with young, underfilled, extensional basins, high-angle normal faults that rupture the surface (Fig. 9) and geomorphic evidence for an east-marching drainage divide. It is not known if the infrequent but large historic earthquakes east of the divide are indicative of new blind normal faults that have nucleated on the detachment, represent active shortening, or alternatively are responding to a different stress field.

Imbricated foredeep and wedge-top basins contain a time-transgressive range of poorly consolidated deposits that span the compressional and extensional regimes. Conceivably, shortening fabrics could be recorded in lithofacies at the base of one of these basins when it was formed and filled in the shortening part of the wedge, only to be superseded by stretching fabrics in overlying lithofacies as the basin was translated westward and into the extending part of the wedge. Adriatic slope transverse rivers (Alvarez, 1999) traverse both the extending and shortening parts of the wedge and contain Pleistocene alluvial deposits representing an AMS geodetic snapshot of the current crustal strains. Published AMS data from the thrust belt show a strike-parallel (NE–SW and horizontal) extension that is perpendicular to compression and shortening directions (Sagnotti, et al., 1998; Caricchi et al., 2016). To confirm these data towards the southeast and to better locate the kinematic transition region between the contracting and extending regions of the overlying Eurasian plate, we sampled AMS data in Oligocene and younger units,

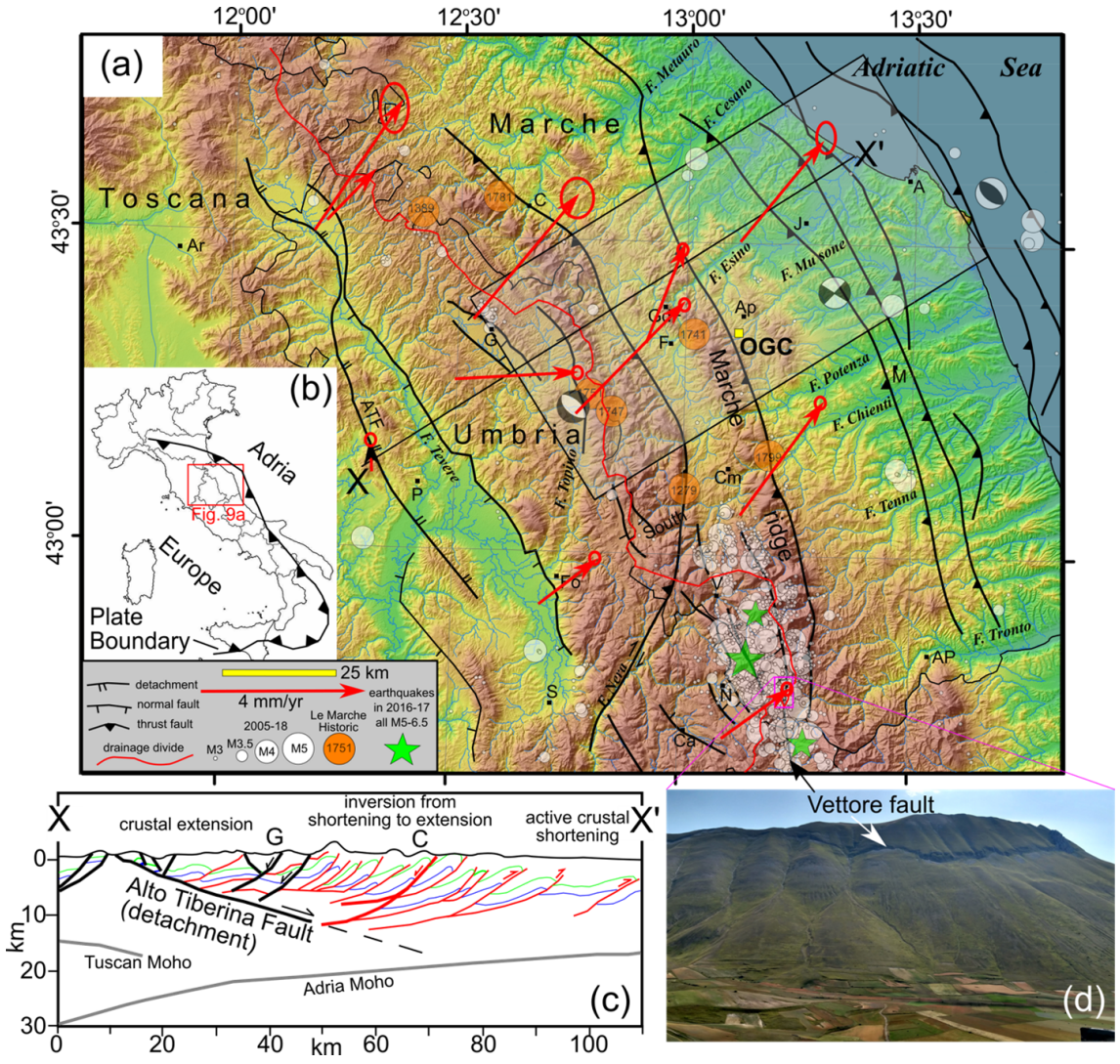

Figure 9. **(a)** Location map showing the topography, known major faults with black lines, the location of large, historic earthquakes in orange circles (from Boncio et al., 1998), the drainage divide as a red line, and GPS geodetic velocities with uncertainties in red arrows (from Hreinsdóttir and Bennett, 2009) in the Northern Apennines showing our research corridor (gray-shaded box). Elevation data are from the TINITALY 10 m digital elevation model (DEM) (Tarquini et al., 2012). Alto Tiberina fault (ATF), Ancona (A), Apiro (Ap), Arezzo (Ar), Ascoli Piceno (AP), Cagli (C), Camerino (Cm), Cascia (Ca), Fabriano (F), Foligno (Fo), Gola di Frasassi (GdiF), Gubbio (G), Jesi (J), Macerata (M), Norcia (N), Osservatorio Geologico Coldigioco (OGC), Perugia (P), Spoleto (S), Visso (V). **(b)** Inset regional map showing the plate boundary and location of Fig. 9a. **(c)** Synthetic cross section of the region in panel **(a)** projected to the X–X' line (modified from Chiaraluce et al., 2017). Normal faults are in black, thrust faults in red, top of Permo-Triassic evaporites in blue, and top of carbonates in green. **(d)** Photo of an exposed bedrock fault scarp from the Umbrian Apennines. Fault scarps are uncommon in most of Marche.

including Quaternary deposits in a NE–SW-oriented corridor across the thrust belt (Fig. 9).

5.2 Methods for Example II

Sampling in the Apennines was designed to identify the location of the modern extensional front. Field collection and specimen preparation occurred as in Example I from Spain, with unconsolidated samples being hardened with sodium silicate before or just after orienting and removal from the outcrop (Fig. 4). We collected samples from 17 sites from sedimentary rocks and poorly consolidated sediments from Late Eocene to late Pleistocene age, with a focus on late Miocene–Pliocene argillaceous marine deposits (Table A1). The Italian specimens were prepared and rock magnetic data were acquired in the Archeomagnetism Laboratory at Centro Nacional de Investigación de la Evolución Humana (CENIEH) (Spain). The AMS of the collected specimens was measured on a MFK1-FA Kappabridge (Agico Instruments), a fully automated inductive bridge, at a frequency of 976 Hz

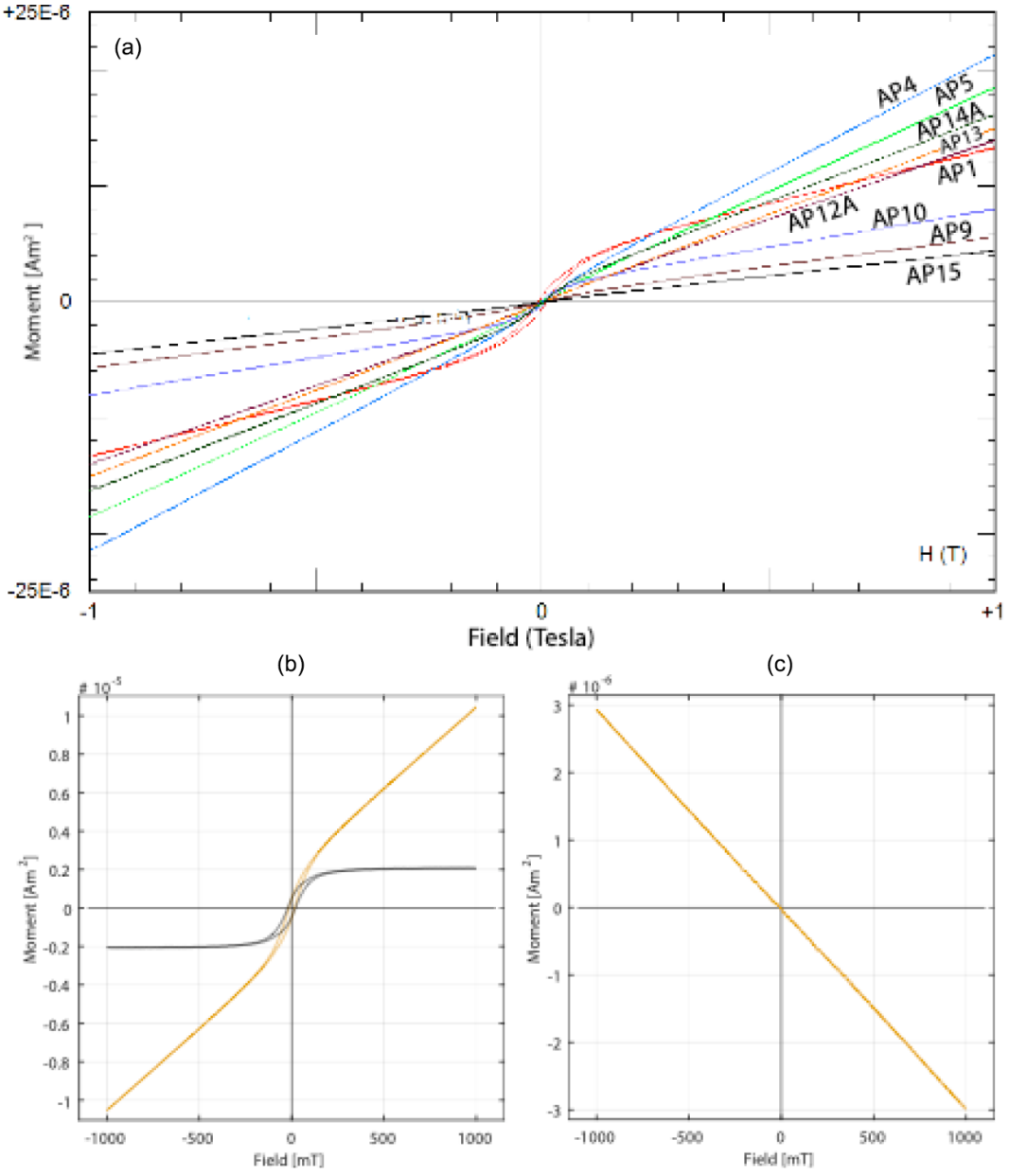

Figure 10. **(a)** Hysteresis curves for representative samples of the studied Apennine range geologic formations (see location in Fig. 10). Paramagnetic susceptibility clearly dominates all the specimens, as revealed by the slope of the loops. **(b)** Example of a specimen where the paramagnetic contribution has been removed in order to enhance the ferromagnetic contribution (loop in black). **(c)** Example of a specimen where diamagnetism dominates the total magnetic susceptibility.

and a field of 200 A m^{-1}. Analysis software (Saphyr6, by Agico) creates a complete susceptibility tensor. Rock magnetic measurements included isothermal remanent magnetization (IRM) acquisition experiments up to 1 Tesla and hysteresis curves to determine the relative contribution of ferromagnetism and paramagnetism to the total susceptibility tensor. These experiments were carried out with a vibrating sample magnetometer (VSM; Micromag 3900).

5.3 Results of Example II

Samples from the Apennines have variable magnetic mineralogy and include a wider range of lithologies and ages than the Betics sampling. Samples from sites AP2 and AP7 (Bisciaro Fm.) are dominated by diamagnetic calcite and negative mean susceptibility, which precludes any meaningful analysis of the AMS axes' orientations. At the 1T field, the magnetization was not fully saturated, indicating the presence of hematite in addition to lower coercivity magnetite as

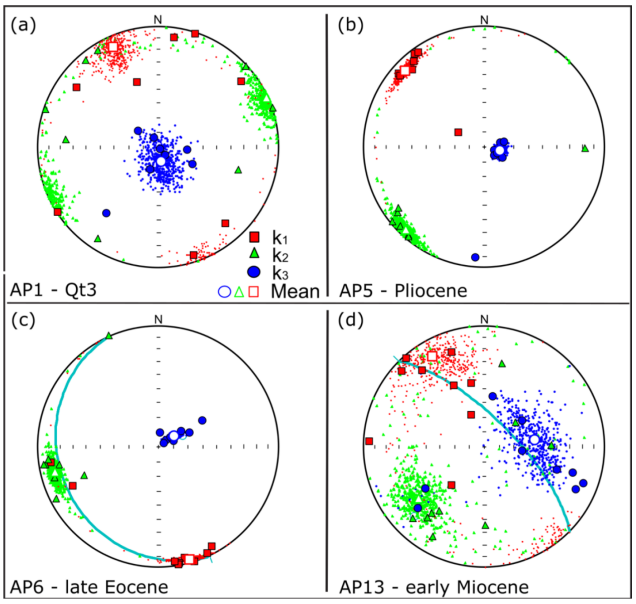

Figure 11. Lower hemisphere stereographic projection of representative sites showing representative fabric patterns in Quaternary deposits **(a)**, older rocks in the Apennine foreland **(b and c)**, and older rocks south of the extensional front **(d)**. The orientation of bedding is shown when not horizontal. Closed symbols indicate measured specimens. Open symbols indicate principal axes orientations with uncertainties.

the dominant ferromagnetic components (Heller, 1978). Still, the bulk magnetic susceptibility is dominated by paramagnetism, as revealed by the hysteresis curves (Fig. 10). The contribution of paramagnetic grains suggests that the measured magnetic fabric can be used as a proxy for phyllosilicate grains' preferred orientation; therefore, the AMS principal axes are indicators of the orientation of the strain axes' orientation (e.g., Soto et al., 2009).

Representative examples of AMS fabrics are shown in Fig. 11. The mean susceptibility shows no positive correlation with the shape parameter or anisotropy degree (T, P_j; Fig. 12). Similar to the data from Spain, the AMS ellipsoids from the Italian specimens indicate low P_j values, revealing a low degree of grain shape preferred orientation and low strains. The AMS axes' distribution is particularly clear in specimens of the argillaceous and semi-consolidated Pliocene Argille Azzurre Fm. At all sites, k_1 axes' orientations are shown as a function of rock formation, as well as the sites at which k_3 is perpendicular to bedding (Fig. 13). All interpretable specimens from the Apennine range samples, including the Pleistocene fluvial deposits, generate a site-mean AMS fabric consistent with contraction and shortening in the wedge.

5.4 Discussion for Example II

The k_1 axis orientation is orthogonal to the rock transport and crustal shortening directions, as recorded in GPS geodesy data and seismology (Fig. 9). Irrespective of sample age, we interpret AMS ellipsoids that have the magnetic lineation in a NW–SE orientation as recording contraction, as this is the main trend of the fault traces and strike of bedding and topography (Fig. 13). A few sites do not provide interpretable kinematic results because the axes directions are scattered and suggest inconsistent strain directions. The calcareous marls of the Bisciaro Fm. (AP2, AP7) have a poorly formed AMS fabric. In these specimens, the mean susceptibility is negative and dominated by diamagnetism, most likely calcite. The absence of a compactional fabric in carbonate-dominated specimens (AP2, AP7) likely indicates that these sediments lithified by cementation soon after deposition.

In general, the distribution of the principal axes of the AMS ellipsoid does not significantly vary with stratigraphic age or structural position. For example, the oldest specimens collected from Eocene–middle Miocene marls and Pliocene siliciclastic rocks (AP6, AP14, AP17) uniformly show AMS fabrics consistent with contractional deformation of the orogenic wedge (Fig. 13), similar to the results of Sagnotti et al. (1998). Most importantly, sites collected from thrust structures that are currently in an extending regime (AP11, AP12, AP13) imply that either the AMS fabric was locked after the original deformation due to the high strain required to rotate grain pairs, or that subsequent extension has not affected the previous AMS fabric (e.g., Larrasoña et al., 2004). The same is true for middle and late Miocene siliciclastic deposits next to the Marche ridge (AP3, AP9), where the current orientations of crustal stresses from fault and earthquake data are ambiguous. Pliocene and Pleistocene samples from near the toe of the orogenic wedge show an orientation consistent with ongoing shortening (AP4, AP5, AP8). Wegmann and Pazzaglia (2009) also report ongoing shortening in this region as evidenced by fluvial terrace folding above the Filottrano thrust, which we cross at the location of AP4.

The kinematic transition zone in central Italy aligns with the topography, the seismicity (Pondrelli et al., 2006), and the GPS geodesy (Bennett et al., 2012; Fig. 9). Our AMS data do not improve on the location of the transition zone because of the lack of samples from Plio-Pleistocene deposits directly northeast of the drainage divide (Fig. 13). Unfortunately, the one Pleistocene river terrace deposit northeast of the divide (AP10) has indeterminate axes. As such, our AMS results are not able to support the idea that there is an apparent rotation of the principal compressive stress between the Adriatic coast and the Marche ridge associated with wedge-scale pore-pressure variations (Peacock et al., 2017). Furthermore, the AMS is unable to determine the stress field responsible for the large historic earthquakes in the region between the drainage divide and the Marche ridge. If earthquakes in the region are related to blind normal faults with tips breaking

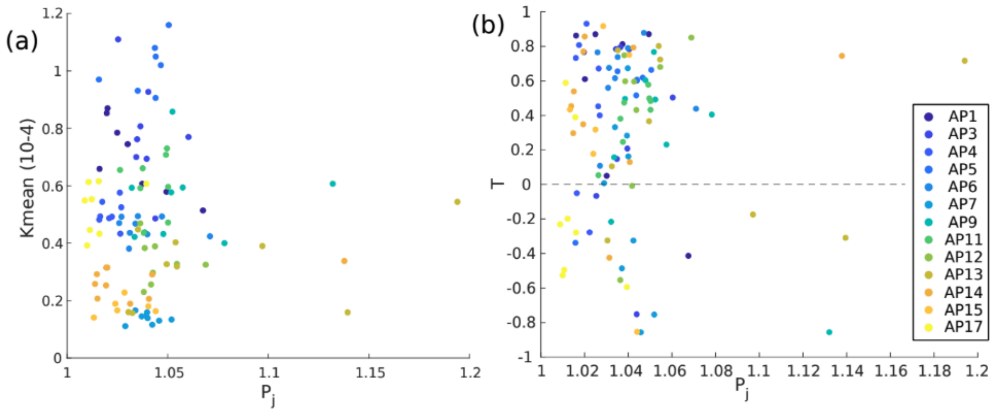

Figure 12. **(a)** Plot of mean susceptibility (K_m) with respect to degree of anisotropy (P_j) for the Apennine specimens. The specimens are color coded by site. **(b)** Jelinek diagram of Apennine specimens, colored by site. All AMS measurements are consistent with low strains (P_j, degree of anisotropy), and nearly all specimens are oblate ($T > 0$).

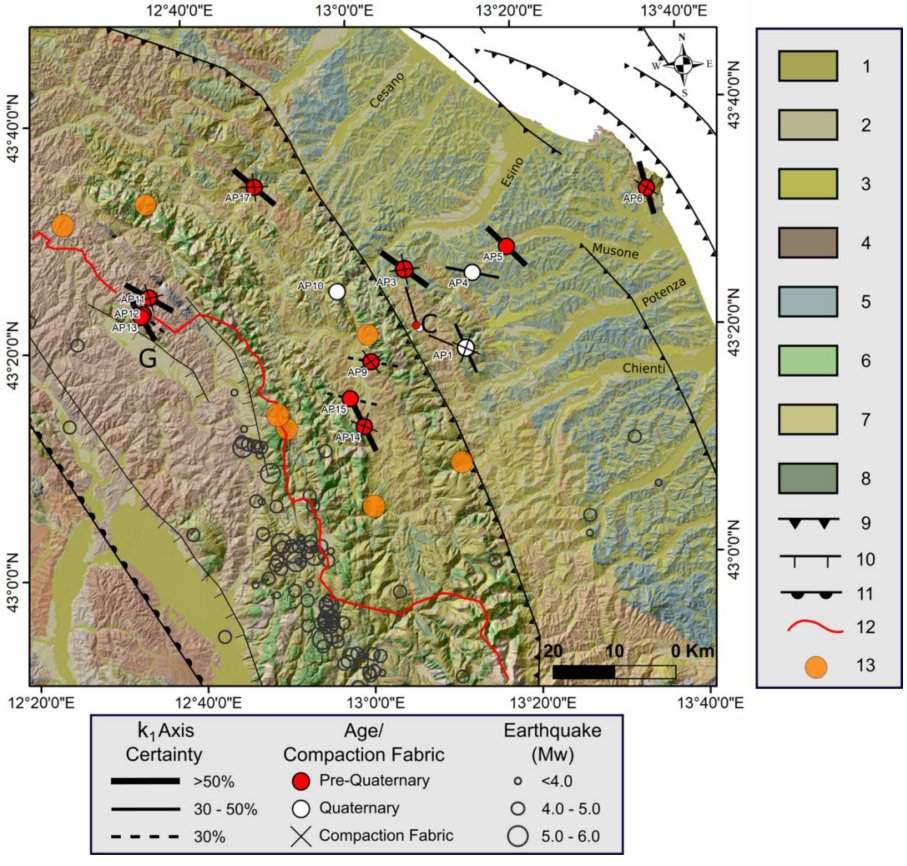

Figure 13. Results of AMS analysis in the Northern Apennines over simplified geology from 1 : 10 000 scale geologic mapping (from Regione Marche and Umbria, http://regione.marche.it, last access: 8 May 2021; http://dati.umbria.it/, last access: 8 May 2021) and topography. Elevation data are from 30 m NASA SRTM JPL combined image data set 2014, distributed by NASA EOSDIS Land Processes DAAC (https://doi.org/10.5067/MEaSUREs/SRTM/SRTMIMGM.003). Extensional earthquake epicenters are compiled from Rovida et al. (2020). The presence of a tectonic fabric was determined by clustering of k_1 declinations outside of the expected compaction fabric. Axis certainty represents the percentage of specimens of the total used to calculate a mean k_1 vector. Right legend: (1) Holocene fill; (2) first-order Quaternary terrace (Q_{t_1}); (3) second-order Quaternary terrace (Q_{t_2}); (4) third-order Quaternary terrace (Q_{t_3}); (5) Argille Azzurre Fm.; (6) Scaglia Rossa Fm.; (7) Maiolica Fm.; (8) Bisciaro Fm.; (9) thrust fault trace; (10) normal fault trace; (11) Alto Tiberina detachment; (12) drainage divide; (13) large historic but pre-instrument earthquakes (pre-1800) of unknown origin (see Fig. 9).

upsection from the Alto Tiberina detachment (Fig. 9), a possible rationale is that, according to extensional critical wedge theory (Davis et al., 1983), a wedge with a taper greater than some critical value is unable to slide over its basal detachment until sufficient wedge thinning on connecting faults reduces the surface slope and wedge taper below the critical value (Xiao et al., 1991). Suitable deposits do outcrop in this critical region, so additional field work and AMS analyses may shed light on this problem.

6 Conclusions

The AMS technique provides an effective way to identify both modern and paleokinematics from sediments and sedimentary rocks largely independent of the magnetic mineralogy of a specimen. Stratigraphically controlled AMS measurements are a deep-time paleogeodetic technique that can be combined with structural geology, GPS geodesy, and seismic data to collectively describe the kinematics of active orogens and to better understand the nature of seismic hazards. In both the Betic Cordillera (Example I) and Northern Apennines (Example II), weak but well-organized penetrative AMS fabrics were recovered from young unconsolidated and unburied rocks that could not be analyzed with more traditional methods. In the Betic Cordillera, we established a long-term consistency to the strain field from the late Miocene to the present from unburied, young deposits around the Sierra Nevada. For the Northern Apennines, all studied sites, regardless of the sites' stratigraphic age, ubiquitously record NW–SE-oriented k_1 axes' orientations, irrespective of structural position. Contractional strains in the most southwest-located samples are likely locked into the rocks and do not record superposed penetrative extension. In any case, the recovered magnetic fabric orientation successfully determined the kinematics of an area near the synorogenic surface in the still-contracting orogen toe region.

Appendix A

Table A1. List of specimens.

Sample	Lat	Long	Elevation (m)	Formation	Age	Composition and texture	Number of specimens
Spain							
SN1	37.04972	−3.64923	853	–	Quaternary	Siliciclastic silt	12
SN3	36.9539	−3.05758	555	–	Quaternary	Siliciclastic silt	15
SN4	36.95832	−2.99537	600	–	Neogene	Siliciclastic silt	11
SN5	37.26138	−3.73503	609	–	Neogene	Siliciclastic silt	9
SN6	37.00809	−2.56091	501	–	Neogene	Siliciclastic sand	12
SN7	37.22960	−3.11414	1037	–	Neogene	Siliciclastic sand	14
Italy							
AP1	43.34778	13.12132	462	Ghiaia Urbisaglia Fm.	Early Pleistocene	Calcareous and siliciclastic silt	8
AP2	43.36193	13.09481	454	Bisciaro Fm.	Early Miocene	Argillaceous marl	8
AP3	43.35226	13.11542	502	Laga Fm.	Late Miocene	Argillaceous silty sand	8
AP4	43.42590	13.23293	217	Qt4 alluvium	Late Pleistocene	Calcareous and siliciclastic silt	8
AP5	43.46141	13.30483	126	Argille Azzurre Fm.	Pliocene	Siliciclastic blue-gray silty clay	7
AP6	43.53607	13.59282	218	Scaglia Variegata Fm.	Late Eocene	Argillaceous marl	9
AP7	43.55456	13.57438	215	Bisciaro Fm.	Early Miocene	Argillaceous marl	9
AP8	43.40956	13.10795	425	Argille Azzurre Fm.	Pliocene	Siliciclastic blue-gray silty clay	8
AP9	43.30225	13.02115	469	Fm. Camerino (Laga Fm.)	Late Miocene	Siliciclastic argillaceous sandy silt	9
AP10	43.40180	12.96773	223	Qt3 alluvium	Middle Pleistocene	Calcareous and siliciclastic silt	9
AP11	43.41049	12.58075	553	Marnosa Arenacea Fm.	Middle Miocene	Siliciclastic argillaceous sandy silt	8
AP12	43.38627	12.56814	638	Marnosa Arenacea Fm.	Middle Miocene	Siliciclastic argillaceous sandy silt	8
AP13	43.38261	12.56343	629	Bisciaro Fm.	Early Miocene	Argillaceous marl	9
AP14	43.20721	13.00143	520	Scaglia Cinerea Fm.	Oligocene	Siliciclastic and calcareous argillaceous sandy silt	10
AP15	43.24922	12.97616	406	Scaglia Cinerea Fm.	Oligocene	Siliciclastic and calcareous argillaceous sandy silt	6
AP16	43.51872	12.72748	500	Scaglia Cinerea Fm.	Oligocene	Siliciclastic and calcareous argillaceous sandy silt	10
AP17	43.56574	12.80247	421	Laga Fm.	Late Miocene	Siliciclastic argillaceous sandy silt	8

Code availability. The Pmagpy code is available at https://earthref.org/PmagPy/cookbook/ (Magnetics Information Consortium, 2020). PmagPy code was used to analyze and plot AMS data. The Anisoft code is available at https://www.agico.com/text/software/anisoft/anisoft.php (AGICO, 2020).

Data availability. The datasets used in this paper are available upon request.

Author contributions. DJA, JMP, and CB conceived the Spanish project and completed sampling, sample preparation, measurement, and analyses. DJA and JMP conceived the Italian project. DJA, FJP, AM, and LKC completed the Italian sampling. DJA and JMP prepared the Italian specimens, measured the samples, and analyzed the results. DJA, FJP, JAF, CB, and KPK analyzed results and drafted figures for the manuscript. DJA and FJP wrote the first draft of the manuscript and edited each subsequent draft. JMP, KPK, CB, and AM edited multiple drafts of the manuscript. DJA completed the final edits.

Competing interests. The authors declare that they have no conflict of interest.

Special issue statement. This article is part of the special issue "Tools, data and models for 3-D seismotectonics: Italy as a key natural laboratory". It is a result of the workshop on "Tools, data and models for 3D seismotectonics: the Italian laboratory over time", Perugia, Italy, 9–10 July 2019.

Acknowledgements. The authors thank Andrea Rodriguez Rubio, Alondra Jimenez Perez, and Isabel Hernando Alonso of CENIEH for laboratory assistance, and the Association "Le Montagne di San Francesco" for logistical support during the sampling campaign in the Umbria–Marche Apennines. Agico is acknowledged for Anisoft software, and Lisa Tauxe is thanked for PmagPy software (Tauxe et al., 2016) used to analyze the AMS data presented here. David J. Anastasio thanks CENIEH and Josep M. Parés for hosting his academic leave during the fall 2019 semester. We thank Dario Biardello and Ruth Soto for their reviews of the manuscript and the topical editor for the journal, Massimiliano Porreca, for his review.

Review statement. This paper was edited by Massimiliano Porreca and reviewed by Dario Bilardello and Ruth Soto.

References

Advanced Geoscience Instruments Company (AGICO): Anisoft – Advanced Treatment of Magnetic Anisotropy Data, available at: https://www.agico.com/text/software/anisoft/anisoft.php (last access: 18 May 2021), 2020.

Alvarez, W.: Drainage on evolving fold-trust belts: a study of transverse canyons in the Apennines, Basin Res., 11, 267–284, 1999.

Artoni, A.: The Pliocene-Pleistocne stratigraphic and tectonic evolution of the central sector of the Western Periadriatic Basin of Italy, Mar. Petrol. Geol., 42, 82–106, 2013.

Averbuch, O., Delamotte, D. F., and Kissel, C.: Magnetic fabric as a structural indicator of the deformation path within a fold thrust structure – a test case from the Corbieres (NE Pyrenees, France), J. Struct. Geol., 14, 461–474, 1992.

Azañón, J. M, Galve, J. P., Perez-Pena, J. V., Giaconia, F., Carvajal, R., Booth-Rea, G., Jabaloy, A., Vazquez, M., Azor, A., and Roldan, F. J.: Relief and drainage evolution during the exhumation of the Sierra Nevada (SE Spain): Is denudation keeping pace with uplift?, Tectonophysics, 663, 19–32, https://doi.org/10.1016/j.tecto.2015.06.015, 2015.

Bally, A. W., Burbi, L., Cooper, C., and Ghelardoni, R.: Balanced sections and seismic reflection profiles across the central Apennines, Mem. Soc. Geol. Ital., 35, 257–310, 1986.

Barchi, M., De Feyter, A., Magnani, M., Minelli, G., Pialli, G., and Sotera, B.: Extensional tectonics in the Northern Apennines (Italy): evidence from the CROP03 deep seismic reflection line, Mem. Soc. Geol. Ital., 52, 528–538, 1998.

Beccaluva, L., Gabbianelli, G., Lucchini, F., Rossi, P. L., and Savelli, C.: Petrology and K/Ar Ages of volcanics dredged from the Eolian seamounts: Implications for geodynamic evolution of the Southern Tyrrhenian Basin, Earth Pl. Sc. Lett., 74, 187–208, https://doi.org/10.1016/0012-821X(85)90021-4, 1985.

Bennett, R. A., Serpelloni, E., Hreinsdottir, S., Brandon, M. T., Buble, G., Basic, T., Casale, G., Cavaliere, A., Anzidei, M., Marjonovic, M., Minelli, G., Molli, G., and Montanari, A.: Synconvergent extension observed using the RETREAT GPS network, northern Apennines, Italy, J. Geophys. Res., 117, B04408, https://doi.org/10.1029/2011JB008744, 2012.

Bernini, B. M.: The role of transpression movements in the evolution of Neogene basins of the Betic Cordillera, An Tect, 4 ISSN: 0394-5596, 1990.

Biedermann, A. R.: Magnetic Anisotropy in Single Crystals: A Review, Geosciences, 8, 302, 16 pp., https://doi.org/10.3390/geosciences8080302, 2018.

Boccaletti, M., Corti, G., and Martelli, L.: Recent and active tectonics of the external zone of the Northern Apennines (Italy), Int. J. Earth Sci., 100, 1331–1348, https://doi.org/10.1007/s00531-010-0545-y, 2011.

Boncio, P., Lavecchia, G., and Pace, B.: Defining a model of 3D seismogenic sources for Seismic Hazard Assessment applications: the case of central Apennines (Italy), J. Seismol., 8, 407–425, 2004.

Borradaile, G. J.: Magnetic susceptibility,petrofabrics and strain, Tectonophysics, 156, 1–20, https://doi.org/10.1016/0040-1951(88)90279-X, 1988.

Borradaile, G. J. and Henry, B.: Tectonic applications of magnetic susceptibility and its anisotropy, Earth Sci. Rev., 4, 49–93, 1997.

Borradaile, G. J. and Jackson, M.: Anisotropy of magnetic susceptibuility (AMS): magnetic petrofabrics of deformed rocks, in: Magnetic Fabric: Methods and Applications, edited by: Martîn-Hernåndez, F., Lüneburg, C. M. Aubourg, and Jackson, M., Geol. Soc. Spec. Publ., 238, 299–360, 2004.

Borradaile, G. J. and Jackson, M.: Structural geology, petrofabrics and magnetic fabrics (AMS, AARM, AIRM), J. Struct. Geol., 32, 1519–1551, https://doi.org/10.1016/j.jsg.2009.09.006, 2010.

Borradaile, G. J. and Lagroix, F.: The enhancement of magnetic fabrics un high grade gneiss, Geophys. Res. Lett., 27, 2413–2416, https://doi.org/10.1029/2000GL008522, 2000.

Borradaile, G. J. and Tarling, D. H.: The influence of deformation mechanisms on magnetic fabrics in weakly deformed rocks, Tectonophysics, 77, 151–168, 1981.

Borradaile, G. J. and Werner, T.: Magnetic anisotropy of some phyllosilicates, Tectonophysics, 225, 223–248, 1994.

Burmeister, K. C., Harrison, M. J., Marshak, S., Ferre, E, C., and Bannister, R. A.: Comparison of Fry strain ellipse and AMS ellipsoid trends to tectonic fabric trends in very low-strain sandstone of the Appalachian fold-thrust belt, J. Struct. Geol., 9, 1028–1038, 2009.

Caporali, A., Barba, S., Carafa, M. M. C., Devoti, R., Pietrantonio, G., and Riguzzi, F.: Static stress drop as determined from geodetic strain rates and statistical seismicity, J. Geophys. Res., 116, B02410, https://doi.org/10.1029/2010JB007671, 2011.

Caricchi, C., Cifelli, F., Kissel, C., Sagnotti, L., and Mattei, M.: Distinct magnetic fabric in weakly deformed sediments from extensional basins and fold-and-thrust structures in the Northern Apennine orogenic belt (Italy), Tectonics, 35, 238–256, https://doi.org/10.1002/2015TC003940, 2016.

Carminati, E. and Doglioni, C.: Alps vs. Apennines: The paradigm of a tectonically asymmetric Earth, Earth Sci. Rev., 112, 67–96, 2012.

Carrigan, J. H., Anastasio, D. J., Berti, C., and Pazzaglia, F. J.: Post-Messinian Drainage Reorganization in an Active Orogen, Betic Cordillera, Spain, Geol. Soc. Am. Abstract. Prog., 50, ISSN 0016-7592, https://doi.org/10.1130/abs/2018AM-322226, 2018.

Chiaraluce, L., Chiarabba, C., Collettini, C., Piccinini, D., and Cocco, M.: Architecture and mechanics of an active low-angle normal fault: Alto Tiberina Fault, northern Apennines, Italy, J. Geophys. Res., 112, B10310, https://doi.org/10.1029/2007JB005015, 1999.

Chiaraluce, L. Barchi, M. R., Carannante, S., Collettini, C., Mirabella, F., Pauselli, C., and Valoroso, L.: The role of rheology, crustal structures and lithology in the seismicity distribution of the northern Apennines, Tectonophysics, 694, 280–291, 2017.

Cifelli, F., Mattei, M., Hirt, A. M., and Günther, A.: The origin of tectonicmfabrics in "undeformed" clays: the early stages of deformation in extensional sedimentary basins, Geophys. Res. Lett., 31, L09604, https://doi.org/10.1029/2004GL019609, 2004.

Collettini, C.: The mechanical paradox of low-angle normal faults: Current understanding and open questions, Tectonophysics, 510, 253–268, 2011.

D'Agostino, N., Jackson, J. A., Dramis, F., and Funiciello, R.: Interactions between mantle upwelling, drainage evolution and active normal faulting: an example from the central Apennines (Italy), Geophys. J. Int., 147, 475–497, 2001.

Davis, D., Suppe, J., and Dahlen, F. A.: Mechanics of fold-and-thrust belts and accretionary wedges, J. Geophys. Res., 88, 1153–1172, 1983.

Devoti, R., Riguzzi, F., Cuffaro, M., and Doglioni, C.: New GPS constraints on the kinematics of the Apennines subduction, Earth Planet Sc. Lett., 273, 163–174, 2008.

Doglioni, C., Harabaglia, P., Merlini, S., Mongelli, F., Peccerillo, A. T., and Piromallo, C.: Orogens and slabs vs. their direction of subduction, Earth Sci. Rev., 45, 167–208, 1999.

Duggen, S., Hoernle, K., van den Bogaard, P., Rüpke, L., and Morgan, J. P.: Deep roots of the Messinian Salinity Crisis, Nature, 422, 602–606, https://doi.org/10.1038/nature01553, 2003.

Elter, P., Giglia, G., Tongiorgi, M., and Trevisan, L.: Tensional and compressional area in the recent (Tortonian to present) evolution of the Northern Apennines, B. Geofis. Teor. Appl., 17, 3–18, 1975.

Eva, E., Solarino, S., and Boncio, P.: HypoDD relocated seismicity in northern Apennines (Italy) preceding the 2013 seismic unrest: seismotectonic implications for the Lunigiana-Garfagnana area, B. Geofis. Teor. Appl., 55, 739–754, 2014.

Fagereng, Å. and Biggs, J.: New perspectives on "geological strain rates" calculated from both naturally deformed and actively deforming rocks, J. Struct. Geol., 125, 100–110, https://doi.org/10.1016/j.jsg.2018.10.004, 2018.

Fernández-Ibáñez, F. and Soto., J. I.: Crustal Rheology and Seismicity in the Gibraltar Arc (western Mediterranean), Tectonics, 27, 18 pp., https://doi.org/10.1029/2007TC002192, 2008.

Fernández-Ibañez, F., Soto, J. I., Zoback, M. D., and Morales, J.: Present-day stress field in the Gibraltar Arc (western Mediterranean), J. Geophys. Res.-Sol. Ea., 112, B08404, https://doi.org/10.1029/2006JB004683, 2007.

Galadini, F. and Galli, P.: Active tectonics in the central Apennines (Italy) – input data for seismic hazard assessment, Nat. Hazards, 22, 225–270, 2000.

Ghisetti, F. and Vezzani, L.: Normal faulting, transcrustal permeability and seismogenesis in the Apennines (Italy), Tectonophysics, 348, 155–168, 2002.

Giaconia, F., Booth-Rea, G., Martínez-Martínez, J. M., Azañón, J. M., Storti, F., and Artoni, A.: Heterogeneous Extension and the Role of Transfer Faults in the Development of the Southeastern Betic Basins (SE Spain), Tectonics, 33, 2467–89, https://doi.org/10.1002/2014TC003681, 2014.

Giaconia, F., Booth-Rea, G., Ranero, C. R., Gràcia, E., Bartolome, R., Calahorrano, A., Lo Iacono, C., Vendrell, M. G., and Cameselle, A. L.: Compressional tectonic inversion of the Algero-Balearic basin: Latemost Miocene to present oblique convergence at the Palomares margin (Western Mediterranean), Tectonics, 34, 1516–1543, https://doi.org/10.1002/2015TC003861, 2015.

Gutscher, M. A., Dominguez, S., Westbrook, G. K., Le Roy, P., Rosas, F., Duarte, J. C., Terrinha, P., Miranda, J. M., Graindorge, D., Gailler, A., Sallares, V., and Bartolome, R.: The Gibraltar Subduction: A Decade of New Geophysical Data, Tectonophysics, 574/575, 72–91, https://doi.org/10.1016/j.tecto.2012.08.038, 2012.

Heller, F.: Rockmagnetic studies of Upper Jurassic limestones from southern Germany, J. Geophys., 44, 525–554, 1978.

Henry, B.: The magnetic zone axis: a new element of magnetic fabric for the interpretation of magnetic lineation, Tectonophysics, 271, 325—331, 1997.

Hill, K. and Hayward, A.: Structural constraints on the Tertiary plate tectonic evolution of Italy, Mar. Petrol. Geol., 5, 2–16, 1988.

Housen, B. A. Richter, C., and van der, Pluijm, B., A.: Composite magnetic anisotropy fabrics: experiments, numerical models,

and implications for the quantification of rock fabrics, Tectonophysics, 220, 1–12, 1993.

Hreinsdóttir, S. and Bennett, R. A.: Active aseismic creep on the Alto Tiberina low-angle normal fault, Italy, Geology, 37, 683–686, https://doi.org/10.1130/G30194A.1, 2009

Hrouda, F.: Magnetic Anisotropy of Rocks and Its Application in Geology and Geophysics, Geophys. Surv., 5, 37–82, https://doi.org/10.1007/BF01450244, 1982.

Jelinek, V.: Characterization of the magnetic fabric of rocks, Tectonophysics, 79, 63–67, 1981.

Kissel, C., Barrier, E., Laj, C., and Lee, T. Q.: Magnetic fabric in "undeormed" marine clays from compressional zones, Tectonics, 5, 769–781, https://doi.org/10.1029/TC005i005p00769, 1986.

Kligfield, R., Owens, W. H., and Lowrie, W.: Magnetic susceptibility anisotropy, strain and progressive deformation in Permian sediments from the Maritime Alps (France), Earth Pl. Sc. Lett., 55, 181–189, https://doi.org/10.1016/0012-821X(81)90097-2, 1981.

Kodama, K. P. and Sun, W.-W.: Magnetic anisotropy as a correction for compaction-caused paleomagnetic inclination shallowing, Geophys. J. Int., 111, 465–469, 1992.

Koulali, A., Ouazar, D., Tahayt, A., King, R. W., Vernant, P., Reilinger, R. E., McClusky, S., Mourabit, T., Davila, J. M., and Amraoui, N.: New GPS constraints on active deformation along the Africa-Iberia plate boundary, Earth Pl. Sc. Lett., 308, 211–217, 2011.

Larrasoaña, J. C., Pueyo, E. L., and Parés, J. M.: An integrated AMS, structural, paleo- and rock-magnetic study of the Eocene marine marls from the Jaca-Pamplona basin (Pyrenees, N Spain); new insights into the timing of magnetic fabric acquisition in weakly deformed mudrocks, Magnetic Fabric: Methods and Applications, edited by: Martín-Hernández, F., Lüneburg, C. M., Aubourg, C., and Jackson, M., Geol. Soc. Sp. Publ., London, 238, 127–143, 2004.

Latta, D. K. and Anastasio, D. J.: Multiple scales of mechanical stratification and décollement fold kinematics, Sierra Madre Oriental foreland, northeast Mexico, Jof. Struct. Geol., 29, 1241–1255, 2007.

Lavecchia, G., Brozzetti, F., Barchi, M., Menichetti, M., and Keller, J.V.:. Seismotectonic zoning in east-central Italy deduced from an analysis of the Neogene to present deformations and related stress fields, Geol. Soc. Am. Bull., 106, 1107–1120, 1994.

Lavecchia, G., Adinolfi, G. M., Nardis, R., Ferrarini, F., Cirillo, D., Brozzetti, F., De Matteis, R., Festa, G., and Zollo, A.: Multidisciplinary inferences on a newly recognized active east dipping extensional system in Central Italy, Terra Nova, 29, 77–89, 2016.

Le Pichon, X. and Angelier, J.: The Hellenic arc and trench system: a key to the neotectonic evolution of the eastern Mediterranean area, Tectonophysics, 60, 1–42, 1979.

Le Pichon, X., Pautot, G., Auzende, J. M., and Olivet, J. L.: La Mediterranee occidentale depuis l'oligocene; scheme d'evolution: The western Mediterranean since the Oligocene; evolutionary scheme, Earth Pl. Sc. Lett., 13, 145–152, 1971.

Lonergan, L.: Timing and kinematics of deformation in the Malaguide Complex, internal zone of the Betic Cordillera, southeast Spain, Tectonics, 12, 460–476, https://doi.org/10.1029/92TC02507, 1993.

Lonergan, L. and White, N.: Origin of the Betic-Rif Mountain Belt, Tectonics, 16, 504–22, https://doi.org/10.1029/96TC03937, 1997.

Magnetics Information Consortium: PmagPy Cookbook, available at: https://earthref.org/PmagPy/cookbook/ (last access: 18 May 2021), 2020.

Mancilla, FdL., Stich, D., Berrocoso, M., Martin, R., Morales, J., Fernandez-Ros, A., Paez, R., and Perez-Pena, A.: Delamination in the Betic Range: Deep structure, seismicity, and GPS motion, Geology, 41, 307–310, 2013.

Martín-Hernandez, F. and Hirt, A. M.: Separation of ferrimagnetic and paramagnetic anisotropies using a high-field torsion magnetometer, Tectonophysics, 337, 209-221, 2001.

Martín-Hernandez, F. and Hirt, A. M.: The anisotropy of magnetic susceptibility in biotite, muscovite and chlorite single crystals, Tectonophysics, 367, 13–28, 2003.

Martín-Hernández, F. and Ferré, E. C.: Separation of paramagnetic and ferrimagnetic anisotropies. A review, J. Geophys. Res.-Sol. Ea., 112, https://doi.org/10.1029/2006JB004340, 2007.

Martínez-Martínez, J. M., Booth-Rea, G., Azañón, J. M., and Torcal, F.: Active transfer fault zone linking a segmented extensional system (Betics, Southern Spain): Insight into heterogeneous extension Driven by Edge Delamination, Tectonophysics, 422, 159–73, https://doi.org/10.1016/j.tecto.2006.06.001, 2006.

Mattei, M., Sagnotti, L., Faccenna, C., and Funiciello, R.: Magnetic fabric of weakly deformed clay-rich sediments in the Italian peninsula: Relationship with compressional and extensional tectonics, Tectonophysics, 271, 107–122, 1997.

Mattei, M., D'Agostino, N., Zananiri, I., Kondopoulou, D., Pavlides, S., and Spatharas, V.: Tectonic evolution of fault-bounded continental blocks: Comparison of paleomagnetic and GPS data in the Corinth and Megara basins (Greece), Solid Earth, 109, B02106, https://doi.org/10.1029/2003JB002506, 2004.

Mazzoli, S. and Helman, M.: Neogene patterns of relative plate motion for Africa-Europe: some implications for recent central Mediterranean tectonics, Geol. Rund, 83, 464–68, 1994.

Milia, A., Turco, E., Pierantoni, P. P., and Schettino, A.: Four-dimensional tectono- stratigraphic evolution of the southeastern Peri-Tyrrhenian Basins (Margin of Calabria, Italy), Tectonophysics, 476, 41–56, https://doi.org/10.1016/j.tecto.2009.02.030, 2009.

Mitra, G. and Sussman, A. J.: Structural evolution of connecting splay duplexes and their implications for critical taper; an example based on geometry and kinematics of the Canyon Range culmination, Sevier Belt, central Utah, J. Struct. Geol., 19, 503–521, 1997.

Papazachos, B. C., Karakostas, V. G., Papazachos, C. B., and Scordilis, E. M.: The geometry of the Wadati-Benioff zone and lithospheric kinematics in the Hellenic arc, Tectonophysics, 319, 275–300, 2000.

Parés, J. M.: How deformed are weakly deformed mudrocks? Insights from magnetic anisotropy, Geol. Soc. Sp., 238, 191–203, 2004.

Parés, J. M. and Dinarès, J.: Magnetic fabric in two sedimentary rock types from the Southern Pyrenees, J. Geomagn. Geoelectr., 45, 193–205, https://doi.org/10.5636/jgg.45.193, 1993.

Parés, J. M. and van der Pluijm, B. A.: Evaluating magnetic lineations (AMS) in deformed rocks, Tectonophysics, 350, 283–298, 2002.

Parés, J. M., van der Pluijm, B., and Dinares-Turell, J.: Evolution of magnetic fabrics during incipient deformation of mudrocks (Pyrenees, northern Spain), Tectonophysics, 307, 1–14, https://doi.org/10.1016/S0040-1951(99)00115-8, 1999.

Parés, J. M., Hassold, N. J. C., Rea, D. K., and van der Pluijm, B. A.: Paleocurrent directions from paleomagnetic reorientation of magnetic fabrics in deep-sea sediments at the Antarctic Peninsula Pacific margin (ODP Sites 1095, 1101), Mar. Geol., 242, 261–269, 2007.

Peacock, C. P., Tavernelli, E., and Anderson, M. W.: Interplay between stress permutations and overpressure to cause strike-slip faulting during tectonic inversion, Terra Nova, 29, 61–70, https://doi.org/10.1111/ter.12249, 2017.

Pialli, G., Barchi, M., and Minelli, G.: Results of the CROP 03 deep seismic reflection profile, Mem. Soc. Geol. Ital., 52, 647 pp., 1998.

Picotti, V. and Pazzaglia, F. J.: A new active tectonic model for the construction of the Northern Apennines mountain front near Bologna (Italy), J. Geophys. Res., 113, B08412, https://doi.org/10.1029/2007JB005307, 2008.

Platt, J. P., Anczkiewicz, R., Soto, J. I., and Kelley, S. P., and Thirlwall, M.: Early Miocene continental subduction and rapid exhumation in the western Mediterranean, Geology, 34, 981–984, 2006.

Platt, J. P., Behr, W. M., Johanesen, K., and Williams, J. R.: The Betic-Rif Arc and its orogenic hinterland: a review, Annu. Rev. Earth Pl. Sc., 41, 313–357, https://doi.org/10.1146/annurev-earth-050212-123951, 2013.

Pondrelli, S., Salimbeni, S., Ekstrom, G., Morelli, A., Gasperini, P., and Vannucci, G.: The Italian CMT dataset from 1977 to the present, Phys. Earth Planet Int., 159, 286–303, https://doi.org/10.1016/j.pepi.2006.07.008, 2006.

Porreca, M. and Mattei, M.: AMS fabric and tectonic evolution of Quaternary intramontane extensional basins in the Picentini Mountains (southern Apennines, Italy), Int. J. Earth Sci., 101, 863–877, 2012.

Porreca, M., Minelli, G., Ercoli, M., Brobia A., Mancinelli, P., Cruciani, F., Giorgetti, C., Carboni, F., Mirabella, F., Cavinato, G., Cannata, A., Pauselli, C., and Barchi, M. R.: Seismic Reflection Profiles and Subsurface Geologyof the Area Interested by the 2016–2017 Earthquake Sequence (Central Italy), Tectonics, 1116–1137, https://doi.org/10.1002/2017TC004915, 2018.

Ramsay, J. G. and Huber, M. I.: The Techniques of Modern Structural Geology, Vol. 1, Academic Press, San Diego, 1984.

Roberts, G. P. and Michetti, A. M.: Spatial and temporal variations in growth rates along active normal fault systems: an example from the Lazio-Abruzzo Apennines, central Italy, J. Struct. Geol., 26, 339–376, 2004.

Rosenbaum, G., Lister, G. S., and Duboz, C.: Reconstruction of the Tectonic Evolution of the Western Mediterranean since the Oligocene, Tectonophysics, 359, 117–129, 2002.

Rovida, A., Locati, M., and Camassi, R.: The Italian earthquake catalogue CPTI15, B. Earthq. Eng., 18, 2953–2984, 2020.

Sagnotti, L. and Speranza, S.: Magnetic fabrics analysis of the Plio- Pleistocene clayey units of the Sant'Arcangelo basin, Southern Italy, Phys. Earth Planet. Inter., 77, 165–176, https://doi.org/10.1016/0031-9201(93)90096-R, 1993.

Sagnotti, L., Speranza, F., Winkler, A., Mattei., and Funiciello, R.: Magnetic fabric of clay sediments from the external northern Apennines (Italy), Phys. Earth Planet. Int., 105, 73–93, 1998.

Sanz De Galdeano, C.: Geologic evolution of the Betic Cordilleras in the Western Mediterranean, Miocene to the present, Tectonophysics, 172, 107–119, https://doi.org/10.1016/0040-1951(90)90062-D, 1990.

Sanz De Galdeano, C. and Vera, J. A.: Stratigraphic record and palaeogeographical context of the Neogene basins in the Betic Cordillera, Spain. Basin Res., 4, 21–36, 1992.

Schwehr, K., Tauxe, L., Driscoll, N., and Lee, H.: Detecting compaction disequilibrium with anisotropy of magnetic susceptibility, Geochem. Geophy. Geosy., 7, Q11002, https://doi.org/10.1029/2006GC001378, 2006.

Soto, J. I., Fernandez-Ibanez, F., Fernandez, M., and Garcia-Casco, A.: Thermal structure of the crust in the Gilbralter Arc: Influence on active tectonicsin the western Mediterranean, Geochem. Geophy. Geosy., 9, 11, https://doi.org/10.1029/2008GC002061, 2008.

Soto, R., Larrasoaña, J. C., Arlegui, L. E., Beamud, E., Oliva-Urcia, B., and Simón, J. L.: Reliability of magnetic fabrics of weakly deformed mudrocks as a palaeostress indicator in compressive settings, J. Struct. Geol., 31, 512–522, 2009.

Stich, D., Serpelloni, E., Mancilla, F. d. L., and Morales, J.: Kinematics of the Iberia – Maghreb plate contact from seismic moment tensors and GPS observations, Tectonophysics, 426, 295–317, https://doi.org/10.1016/j.tecto.2006.08.004, 2006.

Tarling, D. H. and Hrouda, F.: The Magnetic Anisotropy of Rocks, Chapman and Hall, London, UK, 1993.

Tauxe, L., Shaar, R. Jonestrask, L., Swanson-Hysell, N. L., Minnett, R., Koppers, A. A. P., Constable, C., G., Jarboe, N., Gaastra, K., and Fairchild, L.: PmagPy: Software package for paleomagnetic data analysis and a bridge to the Magnetics Information Consortium (MagIC) Database, Geochem. Geophy. Geosy., 17, 2450–2463, https://doi.org/10.1002/2016GC006307, 2016.

Tarquini, S., Vinci, S., Favalli, M., Doumaz, F., Fornaciai, A., and Nannipieri, L.: Release of a 10-m-resolution DEM for the Italian territory: Comparison with global-coverage DEMs and anaglyph-mode exploration via the web, Comp. Geosci., 38, 168–170, https://doi.org/10.1016/j.cageo.2011.04.018, 2012.

Wegmann, K. W. and Pazzaglia, F. J.: Late Quaternary fluvial terraces of the Romagna and Marche Apennines, Italy: Climatic, lithologic, and tectonic controls on terrace genesis in an active orogen, Quaternary Sci. Rev., 28, 137–165, 2009.

Weill, A. B. and Yonkee, A.: Anisotropy of magnetic susceptibility in weakly deformed red beds from the Wyoming salient, Sevier thrust belt: Relations to layer-parallel shortening and orogenic curvature, Lithosphere, 1, 235–256, https://doi.org/10.1130/L42.1, 2009.

Valoroso, L., Chiaraluce, L., Di Stefano, R., and Monachesi, G.: Mixed-mode slip behavior of the Alto Tiberina low-angle normal fault system (Northern Apennines, Italy) through high-resolution earthquake locations and repeating events, J. Geophys. Res.-Sol. Ea., 122, 10220–10240, 2017.

Xiao, H.-B., Dahlen, F. A., and Suppe, J.: Mechanics of extensional wedges, J. Geophys. Res., 96, 10301–10318, 1991.